

Supporting Information

Ultrafast Synthesis of High-Silica Erionite Zeolite with Improved Hydrothermal Stability

Jie Zhu,^a Zhendong Liu,^a Kenta Iyoki,^a Chokkalingam Anand,^a

Kaname Yoshida,^b Yukichi Sasaki,^b Sohei Sukenaga,^c Mariko Ando,^d Hiroyuki Shibata,^c

Tatsuya Okubo^{*a} and Toru Wakihara^{*a}

^a Department of Chemical System Engineering, The University of Tokyo,

7-3-1 Hongo, Bunkyo-ku, Tokyo 113-8656, Japan.

E-mail: okubo@chemsys.t.u-tokyo.ac.jp (T.O.) and wakihara@chemsys.t.u-tokyo.ac.jp (T.W.)

^b Japan Fine Ceramics Center, 2-4-1 Mutsuno, Atsuta-ku, Nagoya 456-8587, Japan

^c Institute of Multidisciplinary Research for Advanced Materials, Tohoku University,

2-1-1 Katahira, Aoba-ku, Sendai 980-8577, Japan

^d Graduate School of Engineering, Tohoku University,

6-6-04 Aramaki, Aoba-ku, Sendai 980-8579, Japan

Contents

1, Experimental Section

1.1 Preparation of ERI zeolites by charge density mismatch method

1.2 Ultrafast synthesis of ERI zeolite without employing the charge density mismatch method

2, Characterisation

3, Supplementary Tables

Table S1 Comparison of C/N ratios of the ERI product and OSDAs

Table S2 Synthesis time and Si/Al ratio of ERI zeolite synthesised under different alkaline conditions

4, Supplementary Figures

Figure S1 Photographs of the reactor as well as the heating tool used for the ultrafast synthesis of ERI zeolite.

Figure S2 N₂ adsorption–desorption isotherms of the conventional and fast-synthesised ERI zeolite.

Figure S3 XRD patterns of ERI zeolite synthesised under different alkaline conditions.

Figure S4 Total structure factors, $S(Q)$, of the conventional and fast-synthesised ERI zeolites.

Figure S5 Pair distribution functions, $G(r)$, of conventional ERI and fast-synthesised ERI.

Figure S6 Hydrothermal stability test results of conventional ERI and fast-synthesised ERI.

1, Experimental section

1.1 Preparation of ERI zeolites by charge density mismatch method

The composition of the initial reactant mixture was as follows: 6.37 TPAOH/1.63 RBr₂/1.43 KOH/0.8 Al₂O₃/16 SiO₂/258 H₂O, where TPAOH and RBr₂ represent tetrapropylammonium and hexamethonium bromide, respectively. The reagents used for the preparation of ERI zeolite included aluminium sec-butoxide (Al[OCH(CH₃)C₂H₅]₃, 97%, Aldrich), tetrapropylammonium hydroxide (TPAOH, 40% aqueous solution, Merck), hexamethonium bromide (TCI), colloidal silica (LUDOX[®] AS-40, 40 wt% suspension) and potassium hydroxide solution (Wako Pure Chemical Industries, Ltd.). Initially, TPAOH solution was used to dissolve aluminium sec-butoxide, followed by the addition of colloidal silica. After homogenisation for 1 h, the reactant mixture was aged for 20 h at 95 °C. To the resulting clear CDM solution, hexamethonium bromide dissolved in de-ionised water was added dropwise. Then, potassium hydroxide solution and de-ionised water were added into the solution followed by stirring for 1 h to form homogenised aluminosilicate reactant. The initial reactant mixture was finally transferred to an autoclave for hydrothermal treatment at 150 °C for 5 days. The solid products were recovered by centrifugation, washed and dried overnight at 80 °C in an oven.

1.2 Ultrafast synthesis of ERI zeolite without employing the charge density mismatch method

The composition of the initial reactant mixture was as follows: 1.63 RBr₂/7.8 KOH/0.8 Al₂O₃/16 SiO₂/258 H₂O, where RBr₂ represents hexamethonium bromide. First, aluminium sec-butoxide was dissolved in KOH solution, followed by the dropwise addition of a solution containing hexamethonium bromide dissolved in de-ionised water.

Colloidal silica and de-ionised water were then added slowly to form an aluminosilicate reactant. The reactant mixture was homogenised for 2 h and aged for 20 h at 90 °C in an oven. To this aluminosilicate mixture, 10 wt% ERI seed crystals synthesised via the CDM method were added, and the resulting reactant was stirred for 10 min prior to the hydrothermal treatment. The quantity of seeds added to the synthesis mixture was based on the amount of SiO₂. Finally, 1.7 g of the reactant mixture was fed into a tubular reactor (4.4 mm inner diameter, 6.6 mm outer diameter, 13.5 cm length) and heated at 210 °C in a preheated oil bath for different periods. The solid products were recovered by centrifugation and dried overnight at 80 °C in an oven.

2, Characterisation

The crystalline phases of all the solid products were identified by a Rigaku Ultima IV X-ray diffractometer using CuK α radiation ($\lambda = 0.15406$ nm, 40 kV, 40 mA) at a scan rate of 4°/min. The crystallinity of the solid product was calculated on the basis of the areas of the peaks ranging from 20° to 30°. The crystal size and morphology of mordenite zeolite were confirmed by scanning electron microscopy (JSM-7000F, JEOL, Japan) at an acceleration voltage of 15 keV. Elemental analysis of the products was carried out using an inductively coupled plasma–atomic emission spectrometer (ICP-AES, iCAP-6300, Thermo) after dissolving the solid products in a potassium hydroxide solution. Nitrogen adsorption–desorption measurements were performed to evaluate the specific surface area of mordenite crystal using Quantachrome Autosorb-iQ2-MP at –196 °C. Prior to the measurements, all samples were preheated at 400 °C for 4 h under vacuum. Solid-state magic angle spinning (MAS) NMR experiments were conducted using a JNM-ECA 500 (JEOL) instrument. ²⁹Si MAS NMR spectra were recorded at 99.37 MHz with

a $\pi/2$ pulse length of 5.0 μs , a recycle delay of 60 s and a spinning frequency of 10 kHz. High-energy X-ray total scattering (HEXTS) measurements were performed on powder samples at the beamline BL04B2 (SPring-8, Japan) with a horizontal two-axis diffractometer. The energy of incident X-ray was 61.43 keV ($\lambda = 0.2018 \text{ \AA}$). The maximum Q ($Q = 4\pi\sin\theta/\lambda$), Q_{max} , collected in this study was 20 \AA^{-1} . The obtained data were subjected to well-established analysis procedures, such as absorption, background and Compton scattering corrections and were subsequently normalised to give a Faber–Ziman total structure factor $S(Q)$. The pair distribution function, $G(r)$, was then calculated using the following function:

$$G(r) = 4\pi r [\rho(r) - \rho_0] = \frac{2}{\rho} \int_{Q_{min}}^{Q_{max}} Q [S(Q) - 1] \sin(Qr) dQ$$

where ρ is the atomic number density (for example, 0.055 \AA^{-3} for Al: 1, Si: 105, O: 212).

3, Supplementary Tables

Table S1. Comparison of C/N ratios of the ERI product and OSDAs

Sample	Chemical Composition	C / N ratio
ERI	-	6.07*
TPAOH	$\text{C}_{12}\text{H}_{29}\text{NO}$	12
Me ₆ -diquat-6	$\text{C}_{12}\text{H}_{30}\text{Br}_2\text{N}_2$	6

*Measured by CNH elemental analysis.

Table S2. Synthesis time and Si/Al ratio of ERI zeolite synthesised under different alkaline conditions

Synthetic conditions	Synthesis time	Si/Al ratio
1.63 RBr ₂ :6.5 KOH: 0.8 Al ₂ O ₃ : 16 SiO ₂ : 258 H ₂ O	4 h	7.6
1.63 RBr ₂ : 7.8 KOH: 0.8 Al ₂ O ₃ : 16 SiO ₂ : 258 H ₂ O	2 h	5.5
1.63 RBr ₂ : 9.1 KOH: 0.8 Al ₂ O ₃ : 16 SiO ₂ : 258 H ₂ O	30 min	4.5
1.63 RBr ₂ : 10.4 KOH: 0.8 Al ₂ O ₃ : 16 SiO ₂ : 258 H ₂ O	20 min	4.1

4, Supplementary Figures

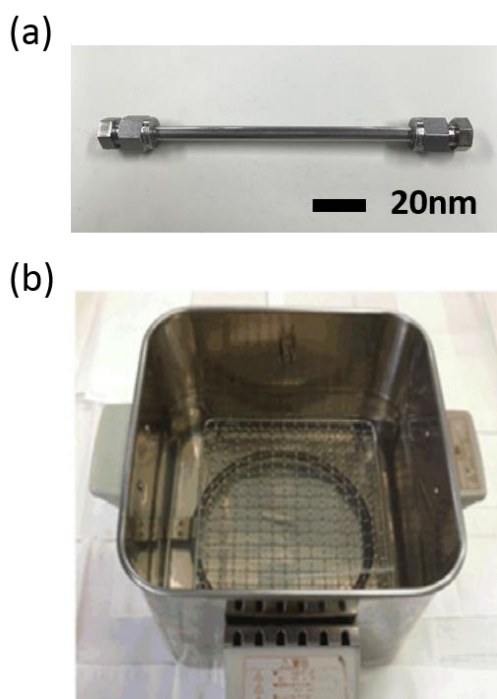


Figure S1. Photographs of the reactor as well as the heating tool used for the ultrafast synthesis of ERI zeolite. (a) the tubular reactor; (b) the pre-heated oil bath.

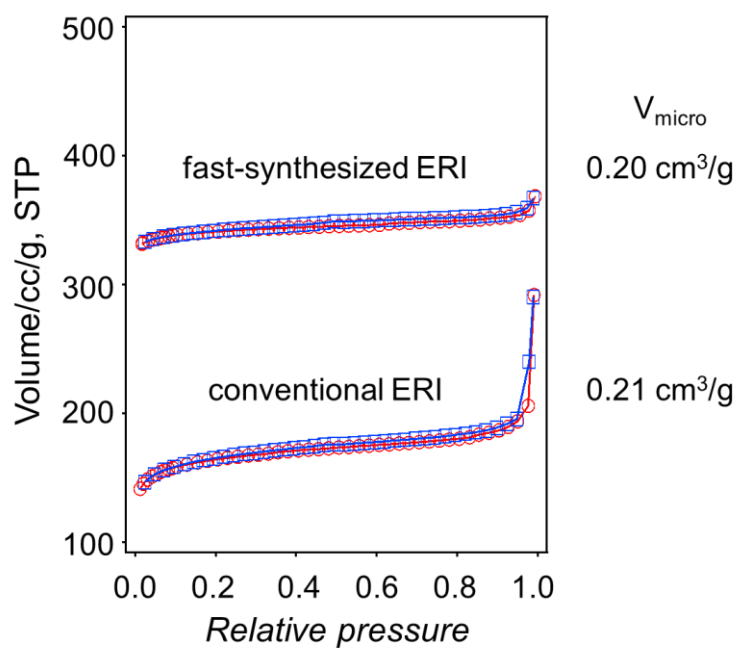


Figure S2. N₂ adsorption–desorption isotherms and micropore volumes of conventional and fast-synthesised ERI zeolites.

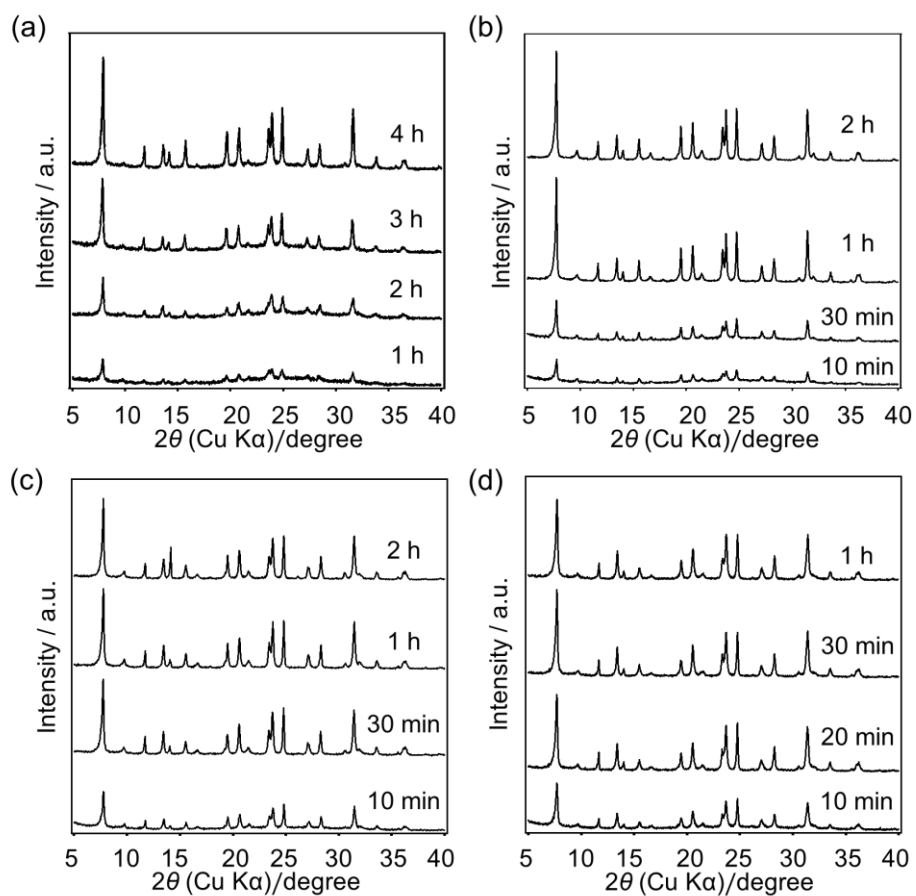


Figure S3. XRD patterns of ERI zeolite synthesised under different alkaline conditions. (a) 1.63 RBr₂: 6.5 KOH: 0.8 Al₂O₃: 16 SiO₂: 258 H₂O; (b) 1.63 RBr₂: 7.8 KOH: 0.8 Al₂O₃: 16 SiO₂: 258 H₂O; (c) 1.63 RBr₂: 9.1 KOH: 0.8 Al₂O₃: 16 SiO₂: 258 H₂O; (d) 1.63 RBr₂: 10.4 KOH: 0.8 Al₂O₃: 16 SiO₂: 258 H₂O. All diffraction peaks are ascribed to ERI zeolite.

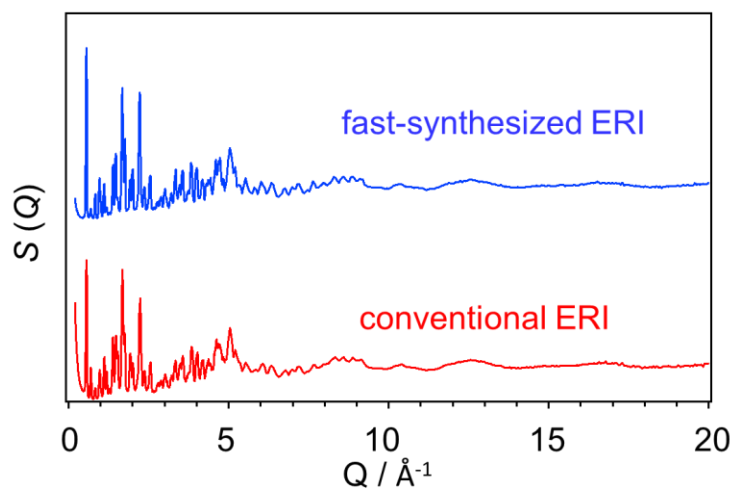


Figure S4. Total structure factors, $S(Q)$, of the conventional and fast-synthesised ERI zeolites.

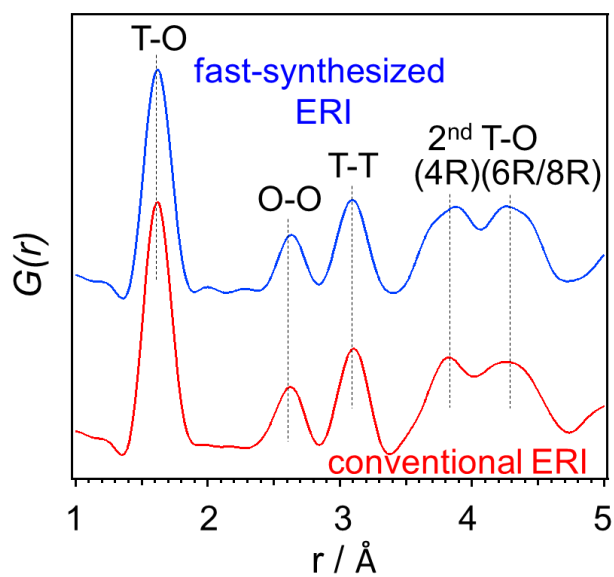


Figure S5. Study of the various atomic distances using high-energy X-ray total scattering (HEXTS). Pair distribution functions, $G(r)$, of conventional ERI and fast-synthesised ERI.

Figure S4 shows the pair distribution function, $G(r)$, of the fast-synthesised ERI and the conventional product. The first peak in the $G(r)$ curves is assigned to the Si–O (ca. 1.61 Å) and Al–O (1.71 Å) distances, and the peaks at 2.6 Å and 3.1 Å are related to the O–O and T–T (T = Si or Al) distances, respectively. The peak observed at 3.7–4.0 Å is mainly attributed to the second nearest T–O of four-membered rings (4R). Similarly, the peak at 4.0–4.5 Å comes from the second T–O distance of 6R and 8R.

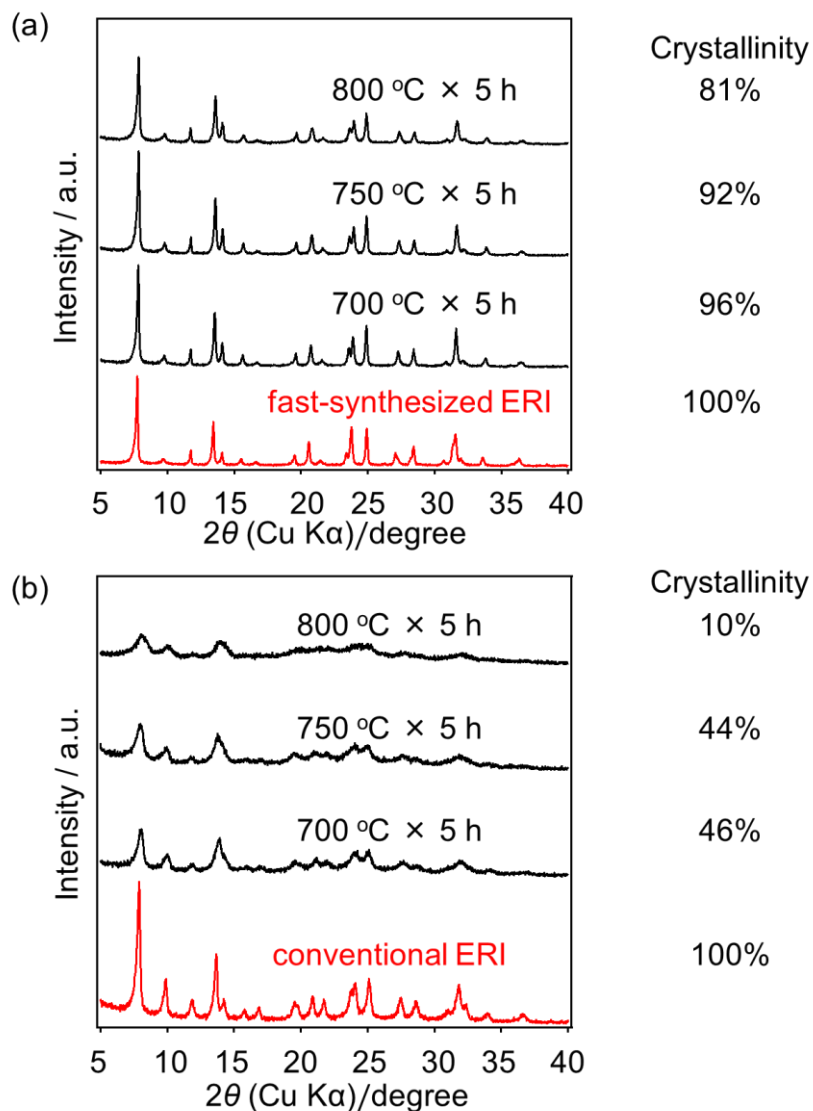


Figure S6. Hydrothermal stability test results. (a) Hydrothermal ageing of fast-synthesised ERI zeolite at 700 °C, 750 °C and 800 °C for 5 h in flowing air containing 10% H₂O. (b) Hydrothermal ageing of conventional ERI zeolite synthesised by the CDM method at 700 °C, 750 °C and 800 °C for 5 h in flowing air containing 10% H₂O. The crystallinity of the solid product was calculated on the basis of the areas of the peaks ranging from 5° to 35°, and ERI samples before hydrothermal ageing were chosen as the standard (100%) for the calculation.